Sapena-Bano, A.; Burriel-Valencia, J.; Pineda-Sanchez, M.; Puche-Panadero, R.; Riera-Guasp, M. (2017). The Harmonic Order Tracking Analysis Method for the Fault Diagnosis in Induction Motors Under Time-Varying Conditions. IEEE Transactions on Energy Conversion. 32(1):244-256. doi:10.1109/TEC.2016.2626008

# The Harmonic Order Tracking Analysis Method for the Fault Diagnosis in Induction Motors Under Time-Varying Conditions

A. Sapena-Bano, J. Burriel-Valencia, M. Pineda-Sanchez, *Member, IEEE*, R. Puche-Panadero, *Member, IEEE*, M. Riera-Guasp, *Member, IEEE*

***Abstract*—This paper introduces a new approach for improving the fault diagnosis in induction motors under time-varying conditions. A significant amount of published approaches in this field rely on representing the stator current in the time-frequency domain, and identifying the characteristic signatures that each type of fault generates in this domain. However, time-frequency transforms produce three-dimensional representations, very costly in terms of storage and processing resources. Moreover, the identification and evaluation of the fault components in the time-frequency plane requires a skilled staff or advanced pattern detection algorithms. The proposed methodology solves these problem by transforming the complex 3D spectrograms supplied by time-frequency tools into simple $x$-$y$ graphs, similar to conventional Fourier spectra. These graphs display a unique pattern for each type of fault, even under supply or load time-varying conditions, making easy and reliable the diagnostic decision even for non-skilled staff. Moreover, the resulting patterns can be condensed in a very small dataset, reducing greatly the storage or transmission requirements regarding to conventional spectrograms. The proposed method is an extension to nonstationary conditions of the harmonic order tracking approach (HOTA). It is introduced theoretically and validated experimentally using commercial induction motors feed through electronic converters.**

*Index Terms*— **Induction machines, fault diagnosis, Hilbert transforms, Fourier transforms, condition monitoring, motor-current signature analysis, broken rotor bar detection, harmonic order tracking analysis, signal processing, transient time-frequency distributions.**

## I. Introduction

SINCE the twentieth century to nowadays, induction motors (IMs) have been increasingly used in a larger number of applications, becoming key elements in the industrial installations. As they acquire greater importance, fault detection is essential to avoid unscheduled outages that would lead to huge economic losses. The most common faults in IMs, their causes and effects are related along the scientific literature [1], [2]. The former techniques developed to detect these faults were based on vibration analysis [3], but motor current signature analysis (MCSA) [4], [5] has been increasingly used for fault diagnosis: each type of fault produces an amplitude modulation in the stator current, with a characteristic frequency, which creates or amplifies harmonics sidebands around the supply frequency in the current energy spectrum. Table I shows the characteristic frequencies of the amplitude modulation ($f_f$) and the sidebands in the stator current spectrum ($f_{sb}$) due to rotor broken bars [6], [7] eccentricity [8], [9], [10] and bearing faults [11], [12],

TABLE I
Fault frequencies

| Fault | Amplitude modulation frequency $f_f = k \cdot f_{f_1}$ | Frequencies of sidebands in the current spectrum $f_{sb} = f_1 \pm f_f$ |
|---|---|---|
| Rotor Broken Bar | $f_f = k \cdot 2sf_1$ | $f_{sb} = f_1 \pm k \cdot 2sf_1$ |
| Mixed eccentricity | $f_f = k \cdot f_r$ | $f_{sb} = f_1 \pm k \cdot f_r$ |
| Bearing outer race | $f_f = k \cdot 0.4N_b f_r$ | $f_{sb} = f_1 \pm k \cdot 0.4N_b f_r$ |
| Bearing inner race | $f_f = k \cdot 0.6N_b f_r$ | $f_{sb} = f_1 \pm k \cdot 0.6N_b f_r$ |

where $k = \pm 1, \pm 2, \pm 3, \ldots$, $f_1$ is the supply frequency, $f_{f_1}$ is the principal fault component of the series, $f_r$ is the frequency of rotation of the rotor, $s$ is the slip, and $N_b$ is the number of bearing balls. MCSA is a non-invasive technique, which requires just a single current sensor for acquiring the stator current signal, and a fast Fourier transform (FFT) for obtaining its energy spectrum, where the fault components can be detected at the frequencies given in Table I. However, MCSA also has an important drawback: it is only suitable for diagnosis of IMs working in steady state. In nonstationary conditions, where $f_1$, $f_r$, and $s$ can change along time in the expressions of Table I, the FFT of the stator current is not able to display the characteristic peaks that reveal the presence of a given fault. Instead, other transforms based on time-frequency distributions (TFD) [6], such as the short time Fourier transform (STFT) [13], the wavelet transform (WT) [14], [15], the Wigner Ville distribution (WVD) [16] or the Gabor transform, [17], among others, have been used to track the fault harmonics given by Table I in the time-frequency plane. These methods can be regarded as an extension of MCSA to transient conditions, designated as transient MCSA (TMCSA).

But TMCSA poses new challenges to the fault diagnosis of IMs. Fault patterns in the time-frequency ($t$-$f$) plane are much more complex than the single frequency peaks that appear in a steady state spectrum. Besides, in machines working under small and random time varying conditions – as in the case of wind turbines– accurate information about the speed is required, because small slip variations produce different patterns in the time-frequency plane. Thus, the

This work was supported by the Spanish "Ministerio de Economía y Competitividad" in the framework of the "Programa Estatal de Investigación, Desarrollo e Innovación Orientada a los Retos de la Sociedad" (Project reference DPI2014-60881-R).

Authors are with the Institute for Energy Engineering, Universitat Politècnica de València, Camino de Vera s/n, 46022, Valencia, Spain.

maintenance staff must be trained in a huge number of fault patterns. To alleviate this problem, other techniques such as the instantaneous frequency (IF) have been proposed in [18] and [19]. Recent researches on diagnosis under nonstationary conditions are focused not only in reducing the number of patterns and representations, but also in facilitating the diagnostic procedure by presenting the results in a plot similar to the FFT spectrum, as in [20], using the polynomial phase transform, or in [21], using the fractional Fourier transform. Another methodology developed in recent years is based on the so called order tracking analysis technique; as explained in [22] this technique "is a frequency analysis method that uses multiples of the running speed (orders) instead of absolute frequencies (Hz) as the frequency base". Conceptually these techniques obtain a spectrum which corresponds to a signal sampled at constant increments of the angular position of an axis instead of sampling at regular time intervals; it is effective for detection of mechanical failures in which disturbances are related to the angular position of an axis. Recently techniques to obtain the spectrum in the angular domain, but based on signals sampled at regular time intervals are being developed (computed order tracking) as [23] where the static eccentricity is detected using the angular domain order tracking analysis (AD-OT), or [24], where the velocity synchronous Fourier transform (VSDFT) is applied to detect bearing faults.

An alternative approach –the harmonic order tracking analysis (HOTA)– has been recently proposed in [25]; it proposes to re-scale the horizontal axis of the current spectra using a non-dimensional unit termed as generalized harmonic order (which is based on the harmonic order $k$ of the expressions of Table I). It is demonstrated that in this way the fault components always appear in the same position within the current spectrum, giving rise to a unique pattern for each type of fault, irrespectively of the supply frequency and load conditions. Besides, this signature is totally defined by a reduced amount of spectral components with integer harmonic order. Thus, it can be stored or transmitted using just a very small number of data. In [26] the HOTA approach was proposed and successfully tested as a suitable technique for fault diagnostic in wind generators. Nevertheless, the HOTA method as proposed in [25], [26] is only suitable for induction machines working in steady state conditions, which makes this approach not suitable for many applications. A first step toward the application of HOTA in non-stationary conditions is proposed in [27], where the bases of transient HOTA methodology are introduced and applied to the diagnosis of rotor asymmetries through the sampling of rotor current in wound rotor induction machines (WRIM) working as generators connected to the network and undergone to slow speed variations. Nevertheless, the HOTA transient approach, as it is introduced in [27] is only feasible for wound rotor induction machines, since it only works suitably with low frequency signals (as the rotor currents) experiencing slow and limited variations. These characteristics make the method appropriate for diagnostic of wind generators using WRIM, but make it unsuitable for a huge amount of industrial applications based on cage motors working in non-stationary conditions.

Unlike the previous commented works [25], [26], [27], this paper introduces for first time the transient HOTA methodology generalized for cage machines working under non-stationary conditions and supplied through variable speed drives, with different control strategies. Unlike [27], the approach is based on measuring stator currents (instead rotor currents), where the frequencies of the fault related components and of the main component are substantially greater than those the rotor currents. This fact makes necessary to introduce a pre-treatment of the stator currents before performing their $t$-$f$ analysis in order to get a spectrogram with the required resolution. For this purpose, this paper introduces a new method of demodulation, which is based on expressing the stator current in the rotor reference frame; it is demonstrated that in the rotor reference frame the frequencies of all components of interest of the stator current appear affected by the slip, acquiring similar values than those obtained when rotor current was measured. An additional advantage of the approach introduced in this paper is that it just needs to know the rotor position in every sampling time instead the rotor speed. This enables to use an encoder instead a speed sensor, simplifying the calculations and improving the system robustness.

Once a high quality spectrogram of transient stator current is obtained, a low computational cost algorithm is proposed, which performs a re-scaling of the transient current spectrograms using the generalized harmonic order as independent variable; it is demonstrated that in the re-scaled spectrogram (HOTA spectrogram), the signature of every type of fault is unique, and does not depend on the way in which the load, the slip or the supply conditions vary along time. Besides, a simple procedure is introduced, which enables to transform these re-scaled spectrogram into $x$-$y$ graphs, where every fault component is characterized by a peak, with an $x$ coordinate equal to its harmonic order, and with an amplitude equal to its average energy along time. In this way, –as in [25]– the proposed method highlights the presence/absence of a given fault in a simple and clear way, enables to assess the severity of the fault, and also enables a complete characterization of the fault patterns, using a very reduced dataset. But it is noticeable that unlike [25], these goals are achieved with IMs working under nonstationary conditions

The structure of this paper is as follows: In Section II the proposed method is theoretically explained. Section III explains the practical procedure for applying the transient HOTA method to detect rotor asymmetries. In Section IV it is experimentally validated in a laboratory test bench using commercial motors with broken bar faults, working under a wide variety of varying supply frequencies and loads and including a sensitivity analysis, for evaluating the ability of the proposed approach to assess the degree of severity of the faults. Finally, Section V summarizes the conclusions of this work.

## II. HARMONIC ORDER TRACKING ANALYSIS OF INDUCTION MOTORS FAULTS IN NONSTATIONARY REGIME

### *A. Conceptual basis*

The proposed method relies on the fact that all the fault

equations of Table I have a common element, the parameter $k$, which characterizes the fault components when a specific kind of fault arises. For a given fault component, this parameter takes an integer value, which does not change even if the supply frequency, the load or its own frequency vary on time. A direct interpretation of $k$ is that it is a parameter that gives the frequency of a fault component in per unit of the frequency of the principal fault component of the series

$$k = \frac{f_f}{f_1} \ . \tag{1}$$

For a given type of fault, $k$ has integer values ($k \in \mathbb{Z}$). Moreover, a more general interpretation of $k$ can be given, considering these integer values as a subset of a real quantity $K$ ($k \subset \mathrm{K}$, $\mathrm{K} \in \mathbb{R}$); in this way, any frequency in the current spectrogram can be characterized by a value of $K$, which can be taken as a new variable (generalized harmonic order), obtained by solving in $k$ the linear relationships of Table I, column 2,

$$f = f_1 + K \cdot f_{f_1} \ (K \in \mathbb{R}) \Longrightarrow f^k = K = \frac{f - f_1}{f_{f_1}}. \tag{2}$$

That is, a new scale of non-dimensional frequencies that replaces the frequency axis, $f^k = \mathrm{K}$, is obtained by a translation of the origin of frequencies to the supply frequency, and a subsequent normalization, dividing by the frequency of the principal fault component of the analyzed fault.

It is noticeable that, if a spectrum or spectrogram of the current is plotted using the new transformed frequency $f^k$, instead of the absolute value of frequency $f$, then the components related with a given fault will be always directly located at the integer values of $K = k \in Z$. Moreover, this will happen irrespectively of the value of supply frequency, the load or the kind of functioning regime (transient or steady state), therefore highlighting the presence or absence of faults in a simple and clear way.

*B. Mathematical justification*

In this section a mathematical justification of the proposed method is given, assuming an ideal IM working in nonstationary conditions.

In an ideal, healthy machine, the stator current can be considered as purely sinusoidal, whose frequency depends on the changes in the supply frequency

$$\begin{aligned} i_{healthy}(t) &= I_m(t)\, cos\left(2\pi \int_0^t f_1(t)\, dt + \psi_0\right) = \\ &= I_m(t)\, cos\left(\int_0^t \omega_1(t)\, dt + \psi_0\right). \end{aligned} \tag{3}$$

In the case of time-varying conditions, a time-frequency analysis is required to identify both the mains and the fault components along the time. Usually, the spectrogram is the tool used for $t$-$f$ analysis. Conceptually, a spectrogram is a representation of the distribution of the signals energy along the $t$-$f$ plane, using a 2D colored plot. As commented in the introduction, there are many techniques for obtaining the spectrogram of a signal. Actually, these techniques are applied to sampled signals, using numerical methods, and considering that the signal remains quasi-stationary under an analyzing window of length $\Delta t$. It is obvious that a reliable diagnostic requires a suitable $t$-$f$ resolution. Thus, it is mandatory to choose a time interval $\Delta t$ small enough, so that the changes in the signal parameters are negligible during each time interval. Therefore, using such small periods of time to compute the current, the signal can be considered as stationary inside every small time interval $[t_{i-1}, t_i]$, where $t_i = i \cdot \Delta t, \ i \in \mathbb{N}$, and the current can be modelled as

$$\begin{aligned} &i_{healthy}(t) = I_{mi}(t)\, cos\big(2\pi f_{1_i} + \psi_{1(i-1)}\big) = \\ &= I_{mi}(t)\, cos\big(\omega_{1_i} t + \psi_{1(i-1)}\big), \ with \ t_{i-1} \le t \le t_i, \end{aligned} \tag{4}$$

where $I_{m_i}$, $f_{1_i}$, $\omega_{1_i}$ are the, amplitude, the frequency and the pulsation in a specific time interval $[t_{i-1}, t_i]$, and $\psi_{1(i-1)} = \omega_{1(i-1)}\Delta t + \psi_{1(i-2)}$.

When the IM is in faulty state, a series of new components appears in the stator current, giving rise to an amplitude modulation of the healthy motor current, with frequencies given by Table I, column 1. Therefore, the faulty current in the time interval $[t_{i-1}, t_i]$ is given by [27]:

$$\begin{aligned} &i_{faulty}(t) = \big[1 + \beta_{fi}\, cos\big(2\pi f_{fi} t + \psi_{f(i-1)}\big)\big] \cdot i_{healthy}(t) = \\ &= \big[1 + \beta_{fi}\, cos\big(\omega_{fi} t + \psi_{f(i-1)}\big)\big] \cdot I_{mi}\, cos\big(\omega_{1i} t + \psi_{1(i-1)}\big) \\ &with\, t_{i-1} \le t \le t_i \ , \end{aligned} \tag{5}$$

where $I_{fi}$ is the amplitude of the fault component and $\beta_{fi} = I_{fi}/I_{mi}$ is the modulation index, both at time $t_i$. Besides, $\omega_{fi} = 2\pi f_{fi} t$, and $\psi_{f(i-1)} = \omega_{f(i-1)}\Delta t + \psi_{f(i-2)}$

Applying elementary trigonometric relations, the faulty current, (5) can be expressed as

$$\begin{aligned} &i_{faulty}(t) = I_{mi}\, cos\big(\omega_{1i} t + \psi_{1(i-1)}\big) + \\ &+ \frac{1}{2} I_{mi} \beta_{fi}\, cos\left(\big(\omega_{1i} + \omega_{fi}\big)t + \psi_{1(i-1)} + \psi_{f(i-1)}\right) + \\ &+ \frac{1}{2} I_{mi} \beta_{fi}\, cos\left(\big(\omega_{1i} - \omega_{fi}\big)t + \psi_{1(i-1)} - \psi_{f(i-1)}\right) \\ &with\, t_{i-1} \le t \le t_i \, . \end{aligned} \tag{6}$$

The second and the third terms of (6) are the fault components, which, for a given time $t_i$ will produce high energy concentration in the spectrogram at the points $[t_i, f_{1i} + f_{fi}], [t_i, f_{1i} - f_{fi}]$. As nonstationary regime is assumed, the patterns produced in the $t$-$f$ plane by the fault components are unpredictable, since $f_1$ and therefore $f_f$ (which depends on $f_1$ and $f_r$) can vary randomly.

On the contrary, if the change of scale (2) is applied for every time $t_i$ in the spectrogram, the transformed frequency of the fault sideband components $\left(f_{sb}^k\right)$ becomes a constant integer number, irrespectively of the supply frequency or speed variations:

$$f_{sb}^k(t_i) = \frac{f_{1i} - f_{sb}(t_i)}{f_{f1i}} = \frac{f_{1i} - \big[f_{1i} - k f_{f1i}\big]}{f_{f1i}} = k \in \mathbb{Z}. \tag{7}$$

Therefore, the patterns of the fault components in the re-

scaled spectrogram are horizontal straight lines, which intercept the vertical axis at integer numbers $k$, even under nonstationary working conditions.

## III. Application Of Harmonic Order Tracking Analysis To The Detection of Rotor Asymmetries in Nonstationary Conditions

The theoretical justification of HOTA given in the previous section is valid for all the faults cited in Table I; however, the diagnostic reliability is directly related to quality of the spectrogram on which (2) is applied; thus, it is advisable to apply some kind of pre-treatment to the transient current signal for optimizing this spectrogram. This pre-treatment depends on the characteristics of the searched fault components and, consequently, on the type of faults to be diagnosed.

This section explains the practical procedure for applying HOTA to the diagnosis of rotor asymmetries in nonstationary conditions; a specific pre-treatment of the signal for this kind of fault is introduced. This section also introduces two graphical tools designated as "Averaged HOTA Spectrum" (AHS) and "Condensed HOTA Spectrum" (CHS), which are easily derived from the HOTA spectrogram. They are very helpful for making a reliable diagnostic decision, for quantification of the severity of the fault and for saving resources in the storage and transmission of the fault information. Unlike the pre-treatment procedure, the method for obtaining the AHS and CHS, as well as the shape of these graphs, does not depend on the type of the analyzed fault. Fig. 1 summarizes the proposed practical procedure for applica-tion of HOTA to the diagnosis of rotor asymmetries in IM under nonstationary conditions.

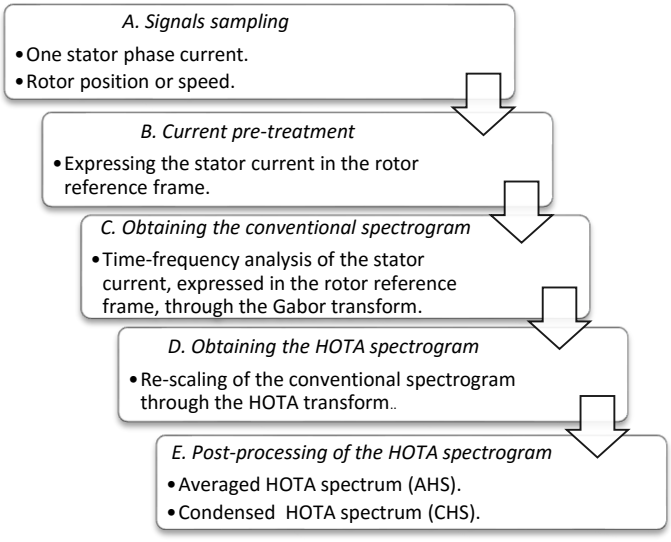


Fig. 1. Scheme for application of HOTA to detection of rotor asymmetries in nonstationary conditions.

For better illustrating the proposed method, several experimental graphs obtained from a test of an IM with one rotor broken bar, supplied through a commercial variable speed drive (VSD), shown in Fig. 2, will be used. All the details of the test are given in Section IV (Table II, test b). During this test the frequency supply was cyclically changed between 45 and 50 Hz every 10 seconds, while the load remained constant. Hence, both frequency and slip continuously changed, giving rise to nonstationary conditions. Fig. 2(a) shows the line current during this test.

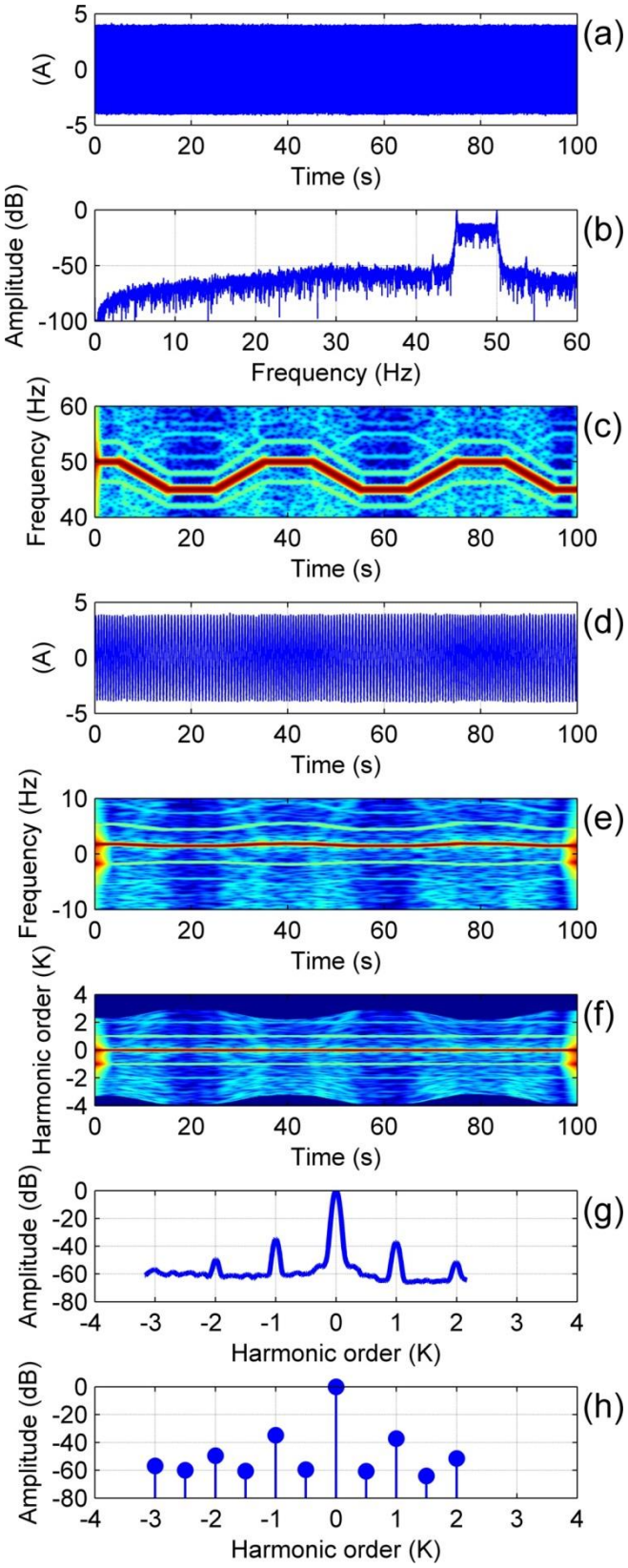


Fig. 2. Example of application of the proposed diagnostic method to an IM with a broken bar. (a) Stator current. (b) Conventional Fourier spectrum of the current in the stator frame. (c) Spectrogram of the current in the stator frame along the time. (d) Stator current in the rotor frame. (e) Spectrogram of the current in the rotor frame. (f) HOTA spectrogram (re-scaled spectrogram) calculated from Fig. 2(e). (g) Averaged HOTA spectrum. (h) Condensed HOTA spectrum.

Fig. 2(b) shows the spectrum of the current using the conventional FFT (MCSA), where, as it can be seen, neither the frequency supply nor the fault components can be identified. Moreover, the mains component evolution hides the fault components. So, TMCSA methods are required.
A detailed explanation of the five blocks (A to E) shown in Fig. 1 is given in the next subsections.

*A. Signals sampling*

A stator phase current is sampled (Fig. 2(a)), and the rotor angular position is measured, either directly (updating the rotor position with the pulses of an encoder, for example), or by integrating the values of a speed sensor.

*B. Current pre-treatment*

The reliability of the diagnosis is directly related with the quality of the spectrogram used as the starting point by the nonstationary HOTA approach. If the amount of stored data, the time interval $\Delta t$, and the analyzed time period T are set, then the frequency resolution of the spectrogram improves as the maximum frequency of the signal decreases.

An effective method to reduce the frequencies of the components of interest of the stator current –in the case of diagnosing rotor asymmetries–, consists in expressing the stator current in the rotor reference frame. This technique leads to a substantial reduction of the frequency of the fundamental and fault-related components, while no changes are introduced in the intrinsic characteristic of the analyzed signal. When the rotor reference frame is used, the expression of the stator current of the ideal faulty machine (6) becomes, as deduced in Annex B,

$$i^r_{faulty}(t) = I_{mi}\cos\big(s_i\omega_{1i}t + \psi_{1(i-1)} - \phi_{rot(i-1)}\big) + \\ + \frac{I_{mi}\beta_{fi}}{2}\cos\Big(\big(s_i\omega_{1i} + \omega_{fi}\big)t + \psi_{1(i-1)} - \phi_{rot(i-1)} + \psi_{f(i-1)}\Big) + \\ + \frac{I_{mi}\beta_{fi}}{2}\cos\Big(\big(s_i\omega_{1i} - \omega_{fi}\big)t + \psi_{1(i-1)} - \phi_{rot(i-1)} - \psi_{f(i-1)}\Big) \\ \text{with } t_{i-1} \le t \le t_i. \qquad (8)$$

Expression (8) shows that, when the rotor frame is used, the fault components also appear as sidebands, separated by the same frequency ($\pm f_f$) from the fundamental component, but with a frequency substantially lower than in the stator reference frame (since $s_i \ll 1$). Thus for the same computational cost, a spectrogram based on (8) allows for a clearer identification of the fault components than that based on (6).

The practical procedure for obtaining the stator current in the rotor reference frame involves the following steps:

- Generating a rotating phasor from the tested stator currents. The rotating phasor can be built in different ways, such as using the Park transform or using the Hilbert Transform ($\mathcal{HT}$). Park's transform needs to measure the three stator phase currents while the $\mathcal{HT}$ just needs to measure a single one. Hence, in this work, the $\mathcal{HT}$ is used due to its lower software and hardware requirements. As explained in [28], the current phasor (or analytic signal) is obtained as a phasor in which the real part equals the phase current, and whose imaginary part is the $\mathcal{HT}$ of the same current

$$\vec{I}(t) = \big[i(t) + j\cdot\mathcal{HT}\big(i(t)\big)\big], \qquad (9)$$

where $\mathcal{HT}(\cdot)$ denotes the Hilbert transform of $(\cdot)$.

- Characterizing the relative position of the stator polar axis related to rotor reference frame; this can be done through the unit phasor $\vec{\phi}_{rot}(t)$, which can be either directly obtained from a encoder signal or integrating the speed signal supplied by a speed sensor,

$$\overrightarrow{\phi}_{rot}(t) = e^{j\phi_{rot}(t)} = e^{j(p\omega_{ri}t + \phi_{rot\,(i-1)})} \\ with\ t_{i-1} < t \le t_i\,, \qquad (10)$$

where $\phi_{rot}(t)$ is the angular position of the rotor (in electrical radians), related to the stator polar axis at time $t$, $\omega_{ri} = 2\pi f_{ri}$ is the mechanical speed of the rotor, in $\mathrm{rad}\cdot\mathrm{s}^{-1}$, $p$ is the number of pole pairs, $s_i$ the slip, and it holds that $\phi_{rot(i-1)} = p\omega_{r(i-1)}\Delta t + \phi_{rot(i-2)}$. $\phi_{rot}(t)$ can be obtained by direct measurement, using an encoder or a resolver, or indirectly recording the speed at each small period of time that is analyzed.

- Obtaining the stator current in rotor coordinates, $i^r(t)$, as the real part of the current phasor in rotor coordinates, that is, projecting this phasor onto the rotor reference axis

$$i^r(t) = Re\big[\vec{I}^r(t)\big] = Re\big[\vec{I}(t)\times\vec{\phi}_{rot}(t)^*\big], \qquad (11)$$

where the superscript $^*$ stands for the complex conjugate.

*C. Obtaining the spectrogram of the stator current expressed in the rotor reference frame*

The spectrogram of the stator current in the rotor reference frame can be calculated through any suitable $t$-$f$ analysis method. Among the different available techniques that were commented in Section I, in this paper the Gabor transform, as introduced in [17], has been selected, since "it allows for the generation of a very high resolution image of the trajectory of the fault components, with the highest concentration in the time–frequency domain" [17].

Fig. 2(c) displays the $t$-$f$ analysis of the stator current expressed in the stator reference frame. The mains component clearly appears oscillating between 45 and 50 Hz. Nevertheless, it is arduous to identify fault components in this representation. On the contrary, Fig. 2(e) shows the spectrogram through Gabor $t$-$f$ analysis of the stator current expressed in the rotor frame (which is plotted in Fig. 2(d)). As it can be seen, the spectral line of the main component is thinner and is less oscillatory than in the stator frame (Fig. 2(c)). Moreover, other spectral lines clearly appear in Fig. 2(e), although it is not possible to assure if they are due to a fault or not, without a further analysis.

*D. Obtaining the re-scaled spectrogram through the HOTA transform (HOTA spectrogram)*

Once the spectrogram of (11) is calculated through the Gabor transform (or any other suitable $t$-$f$ transform), the next step of HOTA is to re-scale the frequency axis in terms of the transformed frequency $f^k$ for every time $t_i$ in the

spectrogram. Particularizing for the rotor asymmetry fault, and using rotor coordinates in (2), the frequency scale transform is defined by

$$f^{r,k}(t_i) = \frac{f_{1i}^r - f_i^r}{f_{f1i}} = \frac{f_{1i}^r - f_i^r}{2sf_{1i}} = \frac{f_{1i}^r - f_i^r}{2f_{1i}^r}, \qquad (12)$$

where the superscript $r$ denotes rotor coordinate. For calculating (12) it is necessary to know the frequency of the fundamental component of the stator current in the rotor reference frame at time $t_i$, $f_{1i}^r$. This value is obtained directly from the spectrogram, as the frequency corresponding to the maximum energy at time $t_i$.

When this transform is applied to a sideband component, the transformed frequency equals to an integer $k$, also when the rotor reference frame is used:

$$f_{sb}^{r,k}(t_i) = \frac{f_{1i}^r - \left(f_{1i}^r - 2ksf_{f1i}\right)}{2f_{1i}^r} = \frac{f_{1i}^r - (f_{1i}^r - 2kf_{1i}^r)}{2f_{1i}^r} = k \in \mathbb{Z}. \qquad (13)$$

Fig. 2(f) shows the re-scaled spectrogram (or HOTA spectrogram). It is remarkable that the fluctuating components of the conventional spectrogram become horizontal straight lines, which intercept the vertical axis at integer values of the transformed frequencies. This fact proves that the detected components are fault components produced by a rotor asymmetry. This set of horizontal lines constitutes a very reliable and easy to identify pattern specifically related to the fault, which avoids the dependence on the variations of the supply frequency, load conditions or speed, thus enabling for a reliable diagnosis, regardless the functioning conditions of the machine.

### *E. Post-processing the HOTA spectrogram*

The HOTA pattern related to the fault is reliable and can be detected even for not skilled staff; nevertheless, it is difficult to assess the severity of the fault, directly from the observation of this pattern. On the other hand, a high resolution spectrogram, as those depicted in Fig. 2(e) and Fig. 2(f), consists of a huge amount of data. Actually, the spectrogram is the graphic representation of an array where the element $A_{ij}$ is the energy of the signal component of frequency $f_j$ at time $t_i$. This array has dimensions $m \times n$, where $m$ is the number of discrete frequencies represented at the spectrogram and $n$ is the number of time intervals. For instance, the spectrogram of Fig. 2(f) contains $10^7$ elements, stored as real numbers. Such a large file size is a drawback for creating historical registers and for transmitting the data to a remote monitoring center.

All these issues are fixed by simply post-processing the HOTA spectrogram for obtaining two new simplified graphs designated as "Averaged HOTA Spectrum" (Fig. 2(e)) and "Condensed HOTA Spectrum" (Fig. 2(f)).

#### *1) The Averaged HOTA Spectrum.*

It is an $x$-$y$ graph, which plots the average value along the sampling period of the signal energy at the transformed frequency $f_j^k$, against this same frequency,

$$A_j\left(f_j^k\right) = \overline{A}_{ij}\left(f_j^k\right) = \frac{1}{n}\sum_{i=1}^{n} A_{ij}\ , \qquad (14)$$

where $A_{ij}$ is the signal energy at time $t_i$ and transformed frequency $f_j^k$, and $A_j$ is the value of the AHS for this frequency.

Fig. 2(g) shows the AHS of the HOTA spectrogram shown in Fig. 2(f), and highlights the power of this method. Formally, this graph is similar to those used in MCSA but using the generalized harmonic order instead the frequency as independent variable. But in the HOTA spectrum the fault components are placed exactly at the integer values of the transformed frequency scale, making easier the interpretation of this graph.

It is noticeable that, for the integer values of the transformed frequency in the horizontal axis, the graph returns the average of the energy of the corresponding fault components throughout the different operating conditions that occur during the sampling time of the current signal. These average values are similar to those calculated through conventional MCSA, and enable for quantification of the severity of the faults. Also, the set of values corresponding integer values of $f^k$ is suitable to be used in advanced artificial intelligence (AI) systems [29], [30], neural networks [31], [32], and support vector machines [33], [34], improving its reliability and reducing the training effort, or used as diagnostic tool by low cost online devices [35] or wireless sensors [36].

Finally, it is remarkable that the file size of the AHS has been drastically reduced regarding the HOTA spectrogram; the AHS consists of *m* real data values, that is, the number of calculated discrete frequencies, ($m = 2000$ data values in the case of Fig. 2(g)), instead of the $m \times n = 10^7$ real data values in the case of Fig. 2(f). This means a reduction of four orders of magnitude in the memory requirements.

#### *2) The Condensed HOTA Spectrum.*

The Condensed HOTA Spectrum (CHS), depicted in Fig. 2(h), is a bar diagram which is built keeping only the values of the AHS of Fig. 2(g) corresponding to the integer values of the generalized harmonic order $K$. Intermediate values have been also included as references, for facilitating the interpretation of the graph. This graph has just 13 values, but contains the same information about the fault than the full length AHS, which has been built using a total number of 2000 values. In this way, from a diagnostic point of view, it is only necessary to store, analyze and/or transmit a single vector of 13 values to assess the motor condition, irrespectively of the sampling frequency, the supply frequency, the load or the machine working conditions. This fact facilitates again the use of low power/low memory devices and low capacity transmission channels.

## IV. Experimental Validation Of The Proposed Method

The tests for validating the proposed method have been performed using a commercial IM with an artificially forced broken bar (Fig. 3). The IM is mounted in a test bench that can reproduce a wide range of working conditions. In this section the main characteristics of the test bench and its

main components are described. Moreover, the experimental tests are depicted and the results are shown and commented.

Fig. 3. Rotor of the tested motor with a forced broken bar fault.

### *A. Test bench*

The test bench is shown in Fig. 4. The IM characteristics are given in Appendix A (machine type II). It is fed through a VSD, model ABB ACS800-01-0005-3+E200+L503, used both in scalar and direct torque control (DTC) modes. A permanent magnet synchronous machine (PMSM), whose main characteristics are given in Appendix A (machine type I), is used as mechanical load. It is controlled by a servo driver, model ABB ACSM1-04AS-024A-4+L516. The servo driver is equipped with a module (FEN21), which outputs an electronically generated software encoder signal with a resolution (programmable) of 720 pulses/revolution. The rotor position has been computed using this signal.

The test bench has been automated using a programmable logic controller (PLC), model ABB PM583 ETH, and a SCADA program. The automation allows to perform the tests in an autonomous way, and makes it possible to reproduce the same test with different IMs, in order to enable a comparative study of the results. The stator current has been measured using a current clamp (20 A, 0-10 kHz, 1 A/100 mV, precision class 2). This clamp has been connected to a digital oscilloscope, model Yokogawa DL750, using an analog voltage input module (ref. 701250, 10 MS, 12 bits). The pulses generated by the VSD software encoder unit are sampled with an input module of the oscilloscope (ref. 701280). A sampling rate of 100 kHz has been used to properly capture the encoder pulses and to avoid the use of anti-aliasing filters; the current signal has been sampled during 100 seconds in each test. Thus, a total number of $10^7$ samples per test have been captured.


Fig. 4. Test bench components and scheme of connections.

### *B. Experimental Tests*

The IM motor with a broken bar fault has been tested covering five nonstationary scenarios, summarized in Table II. These scenarios are characterized by the following parameters:

- The control method in the VSD (scalar or DTC).
- The supply frequency ($f_1$). In two tests the frequency has remained constant, at levels of 25 and 50 Hz. On the contrary, in the other three tests an oscillating frequency with ramps of 10 seconds has been used, changing its values between 20-25 Hz, 45-50 Hz and 40-50 Hz.
- The type of load. As in the case of the supply frequency, in two tests the load level has remained constant at levels of 50% and 70% of rated load. In the other three tests the load has been changed with ramps of 10 seconds between 25-70%, 25-75% and 50-100% of the rated load.

TABLE II
IM FUNCTIONING CONDITIONS DURING THE TESTS

| | Motor controller | Load (type) | Load level (% rated) | $f_1$ (type) | $f_1$ (Hz) |
|---|---|---|---|---|---|
| (a) | Scalar | Constant | 70% | Ramps | 20-25 |
| (b) | Scalar | Constant | 50% | Ramps | 45-50 |
| (c) | DTC | Ramps | 25-70% | Constant | 25 |
| (d) | DTC | Ramps | 25-75% | Constant | 50 |
| (e) | Scalar | Ramps | 50-100% | Ramps | 40-50 |

Fig. 5 shows the results of a conventional $t$-$f$ analysis (Gabor analysis), applied to the currents measured in the five tests described in Table II. In these graphs, the supply frequency is clearly visible. Moreover, other components appear as sidebands close to the mains component. To decide if these lines are due to the broken bar fault, the theoretical frequencies must be computed for each small time interval. Hence, to diagnose the motor, a very precise determination of the supply frequency (which can be obtained in the spectrogram, as the frequency corresponding to the maximum energy for each time $t_i$), and of the rotor speed (which cannot be obtained from the spectrogram), are needed. A slight error in the computation of the position of the fault harmonics (due for example to imprecisions in measuring the speed), can mislead the diagnosis. These problems are even worse for higher order harmonics, with $|k| > 1$, because in these cases the errors in the speed measurement are multiplied by the harmonic order. In addition, a large number of calculations is required to obtain the frequency of the fault sideband in each small range of time. After that, a comparative study between each spectral line evolution and the theoretical calculations would reveal the presence or absence of faults.

The proposed approach is aimed to fix these issues. Following the scheme of Fig. 1, the stator currents are obtained in the rotor frame (Fig. 1, block B). Afterwards, the time frequency analysis through the Gabor transform of these signals (Fig. 1, block C) is performed. Fig. 6 shows the spectrograms of the stator currents in the rotor frame for the five tests described in Table II. Comparing figures 5 and 6 it is noticeable that when rotor reference frame is used, the main component is less oscillatory than in the stator frame, due to the fact that VSD works at near constant slip.

The next step of the proposed approach (Fig. 1, block D)

consists in representing the time-frequency analysis as time-generalized harmonic order analysis (HOTA spectrogram), as shown in Fig. 7. This is done by applying the change of scale given by (12) to the spectrograms of Fig. 6. Figure 7 shows the HOTA spectrograms of the stator current of the tested IM with a broken bar, in the rotor reference frame.

The five HOTA spectrograms of Fig. 7 correspond to the five testing conditions described in Table II. In all cases, the HOTA spectrogram displays the information about the fault in a clear and extremely simple way. It is shown that the spectral line of the mains component remains at the harmonic order $K = 0$. The spectral lines due to rotor broken bar fault are straight horizontal lines and appear at integer harmonic orders $K = k = \pm 1, \pm 2, \pm 3$. This results in a representation which highlights the presence or absence of a fault and it is clear and easy to interpret.

Moreover, it is possible to quantify the diagnostic information contained in the spectrograms of Fig. 7, and to obtain a spectrum as in steady state, by calculating the average of the amplitudes for every value of $K$ along the time, as in Fig. 8. The fault harmonics in the averaged harmonic order spectra are located exactly at the integer harmonic orders values regardless of the working conditions of the motor. This kind of diagram is clearer and easier to interpret than conventional spectrograms. Besides, not only the upper and lower sideband harmonic components (USH and LSH) can be identified quickly in the AHS, but also the fault components with higher order numbers, which improves the diagnosis reliability.

As an additional advantage, from the point of view of the diagnostic process, the only values that are needed to assess the motor condition are the values of the AHS at the integer values of the generalized harmonic order $K$. In this way, the AHS of Fig. 8 can be reduced to just a few values.

Fig. 9 summarizes the condensed HOTA spectra corresponding to the AHS plotted in Fig. 8. Each of these CHS consists of just 13 values (six averaged amplitudes at integer harmonic orders directly related to the fault, and seven amplitudes corresponding to intermediate values of $K$ plotted as reference values). It is noticeable that, as the harmonic order of the fault components remains constant for any working condition of the motor and for any regime (steady or nonstationary), the different five condensed spectra resulting of the testing conditions specified in Table II can be superimposed in a single plot, shown in Fig. 9. This figure shows that the fault information can be always identified at the same position of the harmonic order axis, irrespective of the motor working conditions, the supply frequency and the operating state, which simplifies the process of evaluating the HOTA spectrum in the search of fault signatures.

It is also remarkable that, although the requirements for data storage or data transmission of the condensed spectra are much smaller (five or six magnitude orders) than those

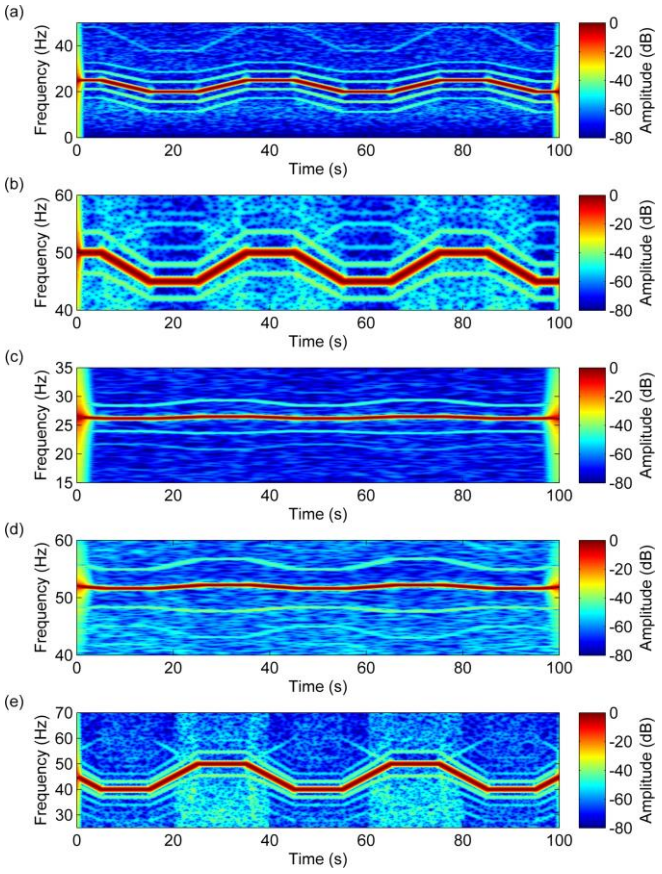


Fig. 5. Gabor analysis of the stator current (in the stator reference frame) of an IM with a broken bar, under the test conditions described in table II: a) Scalar control, constant load (70%), variable frequency (20-25 Hz); b) Scalar control, constant load (50%), variable frequency (45-50 Hz); c) DTC, variable load (25-70%), constant frequency (25 Hz); d) DTC, variable load (25-75%), constant frequency (50 Hz); e) Scalar control, variable load (50-100%) variable frequency (40-50 Hz).

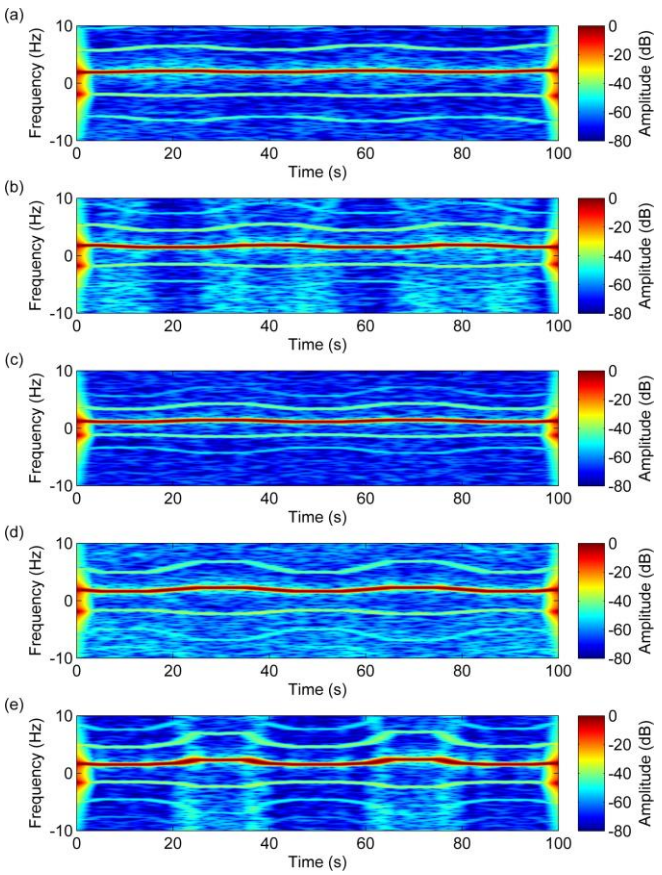


Fig. 6. Gabor analysis of the stator current (in the rotor reference frame) of an IM with a broken bar, under the test conditions described in table II: a) Scalar control, constant load (70%), variable frequency (20-25 Hz); b) Scalar control, constant load (50%), variable frequency (45-50 Hz); c) DTC, variable load (25-70%), constant frequency (25Hz); d) DTC, variable load (25-75%), constant frequency (50 Hz); e) Scalar control, variable load (50-100%) variable frequency (40-50 Hz).

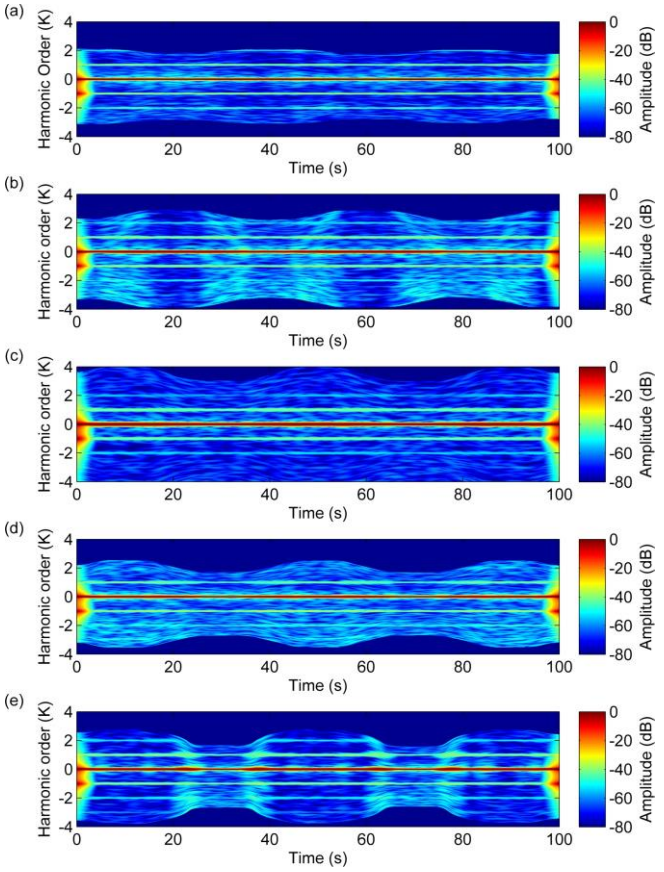


Fig. 7. HOTA spectrograms of the stator current (in the rotor reference frame) of a IM with a broken bar, under the test conditions described in table II: a) Scalar control, constant load (70%), variable frequency (20-25 Hz); b) Scalar control, constant load (50%), variable frequency (45-50 Hz); c) DTC, variable load (25-70%), constant frequency (25Hz); d) DTC, variable load (25-75%), constant frequency (50 Hz); e) Scalar control, variable load (50-100%) variable frequency (40-50 Hz).

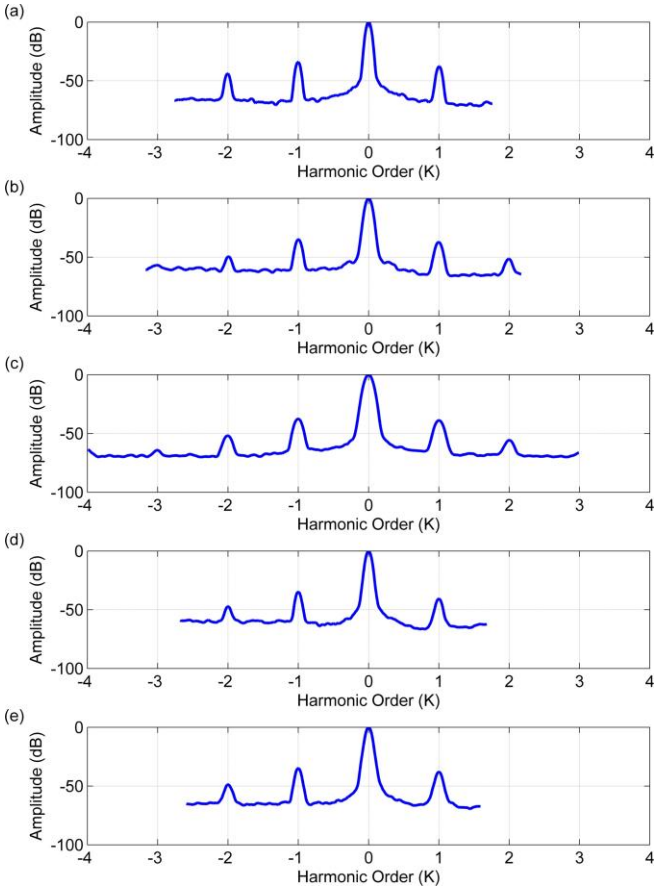


Fig. 8. Averaged HOTA spectra, corresponding to the harmonic order spectrograms depicted in Fig. 7: a) Scalar control, constant load (70%), variable frequency (20-25 Hz); b) Scalar control, constant load (50%), variable frequency (45-50 Hz); c) DTC, variable load (25-70%), constant frequency (25Hz); d) DTC, variable load (25-75%), constant frequency (50 Hz); e) Scalar control, variable load (50-100%) variable frequency (40-50 Hz).

of conventional $t$-$f$ tools, the characterization of the fault is even clearer. These facts constitute clear advantages for making a diagnostic decision by non-skilled staff or by AI based automated diagnostic systems, for elaborating historical registers or for data transmission in remote monitored systems.

### *C. Sensitivity analysis*

In this subsection, the transient HOTA method is applied to an induction cage machine tested under three different fault conditions, in order to verify the ability of the method for assess the degree of severity of the fault. The tests were carried out using the test rig described in section IV, but using a different cage motor, rated 1.1 kW and with two pole pairs, whose characteristics are detailed in Appendix I (Machine Type 3). The tests were performed using one stator and three different rotors, Rotor A in healthy condition, Rotor B with one broken bar and Rotor C with two consecutive broken bars. In this series of tests, the IM was supplied through a VSD with scalar control. The load was keep constant during the test (70%) while the supply frequency cyclically changed between 40 and 50Hz, as is shown in Fig.10(a). Accordingly, the rotor speed also suffered cyclic variations. Figure 10(b) shows the measured evolution of the speed during the tests. The variable frequency profile was programmed in the PLC that controls the test bench, in such a way that all the tests series were

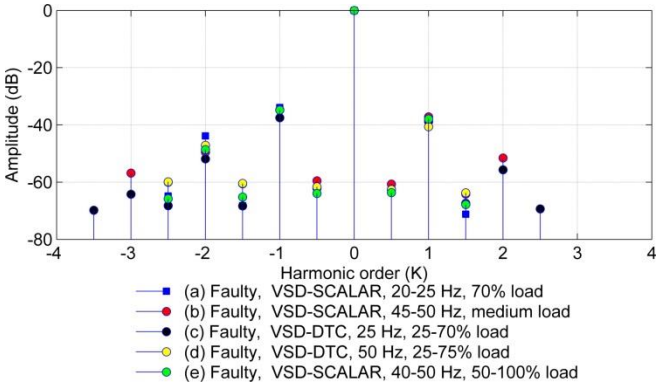


Fig. 9. Superposition in a single plot of the condensed HOTA spectra of the currents in the five tests of Table II.

carried out under the same non-stationary conditions. Once the tests with Rotor A, B, C were performed, the measured stator currents were processed following the scheme of Fig. 1, obtaining finally the averaged HOTA spectra shown in Fig. 11, that correspond to the three tested rotors. These spectra have been superimposed for comparison; in the spectrum of the Rotor A it can be clearly seen two peaks at $K$=-1 and $K$=1, with amplitudes around -55 dB, which correspond to the LSH and USH in healthy condition and inform about the inherent degree of asymmetry of the rotor. It is noticeable that the principal fault components, LSH and USH, placed always exactly at $k$=-1 and $k$=1 respectively

increases more than 18 dB after the first breakage and approximately 6 additional dB after the second breakage. These values are coherent with those found in the technical literature for the LSH amplitude in steady state conditions [37]. An increase of 6 dB for the second bar breakage means that the amplitude of LSH is doubled regarding the case of a simple breakage. This result is very near to the theoretical ratio of 1.8 between LSH amplitudes in the case of double and a single breakage, calculated as in [38], for a machine with two pole pairs and 28 rotor bars.

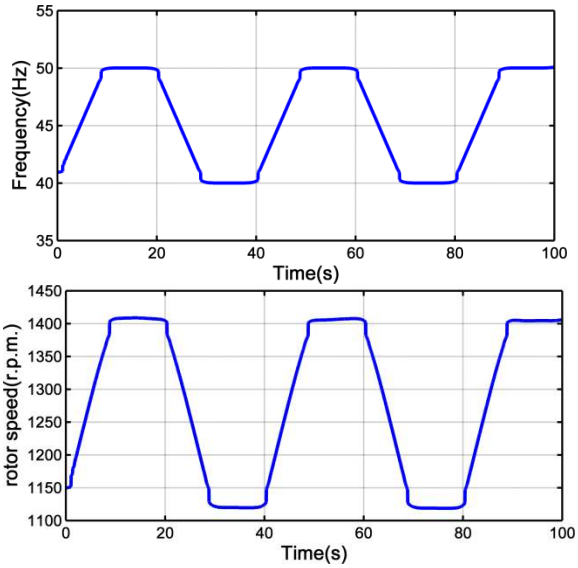


Fig. 10. Evolution of the supply frequency and speed during the sensibility tests.

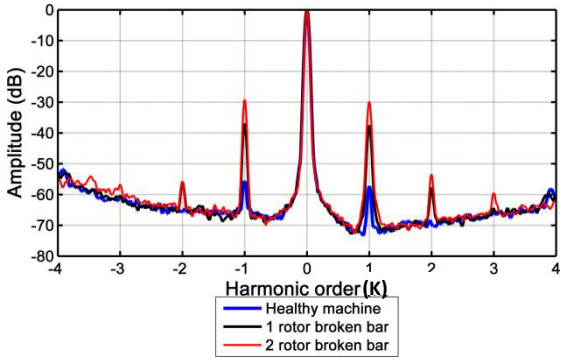


Fig. 11. Averaged HOTA spectrum obtained for the tests of machine type 3, under non stationary conditions shown in Fig.10, for three fault conditions: Healthy, one broken bar, two consecutive broken bars.

## V. Conclusion

This paper introduces a methodology for improving the diagnosis of faults in IMs working under nonstationary conditions. The proposed method relies in a low computational cost transform, which re-scales the frequency axis of the spectrograms resulting from time-frequency analysis, which are commonly used for diagnosing electrical machines in nonstationary conditions. For this purpose, a new variable, designated as "generalized harmonic order" is introduced.

It is demonstrated that the proposed method leads to significant advantages regarding to other time-frequency approaches described at the technical literature. First, after applying the proposed transform, the patterns of the fault related components in the re-scaled spectrograms are unique, and do not depend on the way in which supply frequency, load and rotor speed vary during the testing periods. Moreover, these patterns are very simple and easy to identify: just horizontal straight lines which intercept the transformed frequency axis at integer values. These characteristics enable for a reliable diagnosis even for nonskilled staff, and simplify the development of automatized diagnostic methods based on AI algorithms. Second, from the re-scaled spectrogram, two new low computational cost diagnostic tools have been introduced: the averaged HOTA spectrum and the condensed HOTA spectrum. The AHS is an $x$-$y$ graph similar to a conventional Fourier spectrum, but with the advantage that the peaks representing the fault components are placed always at the same position, irrespectively of the functioning conditions, and, also, the amplitude of these peaks directly give the average energy of the fault components during the testing period. The CHS summarizes the relevant information about the machine condition in a set of less than 20 real numbers, unlike the conventional spectrograms, whose size frequently amounts to more than $10^6$-$10^7$ real data values. These tools make more simple and reliable the diagnostic decision, enable for an easy quantification of the fault severity, and drastically reduce the needs of memory for creating historical registers and the needs of bandwidth for transmitting the machine condition data in remote monitoring systems.

## Appendix A

Machine type I: Permanent magnet synchronous machine. Rated characteristics: $P$ = 4.9 kW, $f$ = 200 Hz, $T$ =15.5 Nm, $I$=14.4 A, and $n$ = 3000 rpm.

Machine type II: Three-phase induction motor, star connection. Rated characteristics: $P$ = 1.5 kW, $f$ = 50 Hz, $U$ =400 V, $I$=3.25 A, and $n$ = 2860 rpm, and $\cos\varphi = 0.85$.

Machine type III: Three-phase induction motor, star connection. Rated characteristics: $P$ = 1.1 kW, $f$ = 50 Hz, $U$ =400 V, $I$=2.25 A, $n$ = 1410 rpm, and $\cos\varphi = 0.85$, 2 pole pairs, 28 rotor bars.

## Appendix B: Expression of the Stator Faulty Current in the Rotor Reference Frame

The first step is to obtain a rotating space vector from the stator currents of the faulty machine. As commented in Section III, this will be done through the $\mathcal{HT}$, building the analytic signal. Substituting (9) in (12) and applying $\mathcal{HT}$ properties, as demonstrated in [24],

$$\begin{aligned}\vec{I}_{\text{faulty}}(t) &= I_{mi}\, e^{\omega_{1i}t+\psi_{1(i-1)}} + \\ &+\frac{1}{2} I_{mi}\beta_{fi}\, e^{j\left((\omega_{1i}+\omega_{fi})t+\psi_{1(i-1)}+\psi_{f(i-1)}\right)} + \\ &+\frac{1}{2} I_{mi}\beta_{fi}\, e^{j\left((\omega_{1i}-\omega_{fi})t+\psi_{1(i-1)}-\psi_{f(i-1)}\right)} \\ &\text{with } t_{i-1} \le t \le t_i\,, \end{aligned} \tag{B1}$$

that is,

$$\vec{I}_{\text{faulty}(t)} = \left(1+\frac{\beta_{fi}}{2}\left(e^{j\left(\omega_{fi}t+\psi_{f_{i-1}}\right)}+e^{-j\left(\omega_{fi}\,t+\psi_{f_{i-1}}\right)}\right)\right)\times \\ \times\; I_{mi}\, e^{j\left(\omega_{1i}+\psi_{1(i-1)}\right)}\,. \tag{B2}$$

Taking into account that

$$p\omega_{ri} = (1 - s_i)\omega_{1i}\,, \tag{B3}$$

where $s_i$ is the slip at $t = t_i$ , and substituting (B3) in (12), the unit vector $\vec{\phi}_{rot}(t)$, which determines the position of the rotor reference frame becomes

$$\vec{\phi}_{rot}(t) = e^{j\left((1-s_i)\omega_{1i}t+\phi_{rot(i-1)}\right)} \text{ with } t_{i-1} \le t \le t_i. \tag{B4}$$

The current phasor expressed in the rotor frame is given by

$$\vec{I}^r(t) = \vec{I}(t) \times \vec{\phi}_{rot}(t)^*, \tag{B5}$$

so, substituting (B1) and (B4) in (B5) gives

$$\begin{aligned}\vec{I}_{\text{faulty}}(t) &= \left(1 + \frac{\beta_{fi}}{2}\left(e^{j\left(\omega_{fi}t+\psi_{f_{i-1}}\right)} + e^{-j\left(\omega_{fi}t+\psi_{f_{i-1}}\right)}\right)\right) \times \\ &\times I_{mi}\, e^{j(\omega_{1i}+\psi_{1(i-1)})} \times e^{-j\left((1-s_i)\omega_{1i}t+\phi_{rot(i-1)}\right)} = \\ &= \left(1 + \frac{\beta_{fi}}{2}\left(e^{j\left(\omega_{f_i}t+\psi_{f_{i-1}}\right)} + e^{-j\left(\omega_{f_i}t+\psi_{f_{i-1}}\right)}\right)\right) \times \\ &\times I_{mi}\, e^{j\left(s_i\omega_{1i}t+\psi_{1(i-1)}-\phi_{rot(i-1)}\right)},\end{aligned} \tag{B6}$$

and, taking the real part of (B6), gives

$$\begin{aligned}&i^r_{faulty}(t) = Re\left[\vec{I}^r_{\text{faulty}}(t)\right] = \\ &= I_{mi}\cos\left(s_i\omega_{1i}t + \psi_{1(i-1)} - \phi_{rot(i-1)}\right) + \\ &+ \frac{I_{mi}\beta_{fi}}{2}\cos\left(\left(s_i\omega_{1i} + \omega_{fi}\right)t + \psi_{1(i-1)} - \phi_{rot(i-1)} + \psi_{f_{i-1}}\right) \\ &+ \frac{I_{mi}\beta_{fi}}{2}\cos\left(\left(s_i\omega_{1i} - \omega_{fi}\right)t + \psi_{1(i-1)} - \phi_{rot(i-1)} - \psi_{f_{i-1}}\right),\end{aligned} \tag{B7}$$

which is the expression used in (8).

## REFERENCES


[1] H. Henao, G. A. Capolino, M. Fernandez-Cabanas, F. Filippetti, C. Bruzzese, E. Strangas, R. Pusca, J. Estima, M. Riera-Guasp and S. Hedayati-Kia, "Trends in Fault Diagnosis for Electrical Machines: A Review of Diagnostic Techniques," *IEEE Ind. Electron. Mag*, vol. 8, no. 2, pp. 31-42, June 2014.

[2] M. Riera-Guasp, J. Antonino-Daviu and G.-A. Capolino, "Advances in Electrical Machine, Power Electronic, and Drive Condition Monitoring and Fault Detection: State of the Art," *IEEE Trans. Ind. Electron.*, vol. 62, no. 3, pp. 1746-1759, March 2015.

[3] P. Henriquez, J. Alonso, M. Ferrer and C. Travieso, "Review of Automatic Fault Diagnosis Systems Using Audio and Vibration Signals," *IEEE Trans. Syst., Man, Cybern., Syst*, vol. 44, no. 5, pp. 642-652, May 2014.

[4] J.-H. Jung, L. Jong-Jae and B.-H. Kwon, "Online Diagnosis of Induction Motors Using MCSA," *IEEE Trans. Ind. Electron.*, vol. 53, no. 6, pp. 1842-1852, Dec. 2006.

[5] S. Lee, D. Hyun, T. Kang, C. Yang, S. Shin, H. Kim, S. Park, T. Kong and H. Kim, "Identification of False Rotor Fault Indications Produced by Online MCSA for Medium-Voltage Induction Machines," *IEEE Trans. Ind. Appl.*, vol. 52, no. 1, pp. 729-739, Jan. 2016.

[6] V. Ghorbanian and J. Faiz, "A survey on time and frequency characteristics of induction motors with broken rotor bars in line-start and inverter-fed modes," *Mechanical Systems and Signal Processing*, Vols. 54-55, pp. 427-456, 2015.

[7] R. Romero-Troncoso, A. Garcia-Perez, D. Morinigo-Sotelo, O. Duque-Perez, R. Osornio-Rios and M. Ibarra-Manzano, "Rotor unbalance and broken rotor bar detection in inverter-fed induction motors at start-up and steady-state regimes by high-resolution spectral analysis," *Electric Power Systems Research* , vol. 133, pp. 142-148, 2016.

[8] J. Faiz and S. Moosavi, "Eccentricity fault detection - From induction machines to DFIG - A review," *Renewable and Sustainable Energy Reviews* , vol. 55, pp. 169-179, 2016.

[9] C. Di, X. Bao, H. Wang, Q. Lv and Y. He, "Modeling and Analysis of Unbalanced Magnetic Pull in Cage Induction Motors With Curved Dynamic Eccentricity," *IEEE Trans. Magn.*, vol. 51, no. 8, pp. 1-7, Aug. 2015.

[10] M. Ojaghi and S. Nasiri, "Modeling Eccentric Squirrel-Cage Induction Motors With Slotting Effect and Saturable Teeth Reluctances," *IEEE Trans. Energy Convers.*, vol. 29, no. 3, pp. 619-627, Sept. 2014.

[11] Z. Gao, C. Cecati and S. Ding, "A Survey of Fault Diagnosis and Fault-Tolerant Techniques - Part I: Fault Diagnosis With Model-Based and Signal-Based Approaches," *IEEE Trans. Ind. Electron.*, vol. 62, no. 6, pp. 3757-3767, June 2015.

[12] V. Leite, J. Borges da Silva, G. Cintra Veloso, L. Borges da Silva, G. Lambert-Torres, E. Bonaldi and L. De Lacerda de Oliveira, "Detection of Localized Bearing Faults in Induction Machines by Spectral Kurtosis and Envelope Analysis of Stator Current," l*EEE Trans. Ind. Electron.*, vol. 62, no. 3, pp. 1855-1865, Mar. 2015.

[13] E. Cabal-Yepez, A. Garcia-Ramirez, R. Romero-Troncoso, A. Garcia-Perez and R. Osornio-Rios, "Reconfigurable Monitoring System for Time-Frequency Analysis on Industrial Equipment Through STFT and DWT," *IEEE Trans. Ind. Informat.*, vol. 9, no. 2, pp. 760-771, May 2013.

[14] P. Konar and P. Chattopadhyay, "Multi-class fault diagnosis of induction motor using Hilbert and Wavelet Transform," *Applied Soft Computing* , vol. 30, pp. 341-352, 2015.

[15] Y. Gritli, S. B. Lee, F. Filippetti and L. Zarri, "Advanced Diagnosis of Outer Cage Damage in Double-Squirrel-Cage Induction Motors Under Time-Varying Conditions Based on Wavelet Analysis," *IEEE Trans. Ind. Appl.*, vol. 50, no. 3, pp. 1791-1800, May 2014.

[16] A. Martinez-Herrera, L. Ledesma-Carrillo, M. Lopez-Ramirez, S. Salazar-Colores, E. Cabal-Yepez and A. Garcia-Perez, "Gabor and the Wigner-Ville transforms for broken rotor bars detection in induction motors," in *Electronics, Communications and Computers (CONIELECOMP), 2014 International Conference on*, Puebla, 2014, pp. 83-87 .

[17] M. Riera-Guasp, M. Pineda-Sanchez, J. Perez-Cruz, R. Puche-Panadero, J. Roger-Folch and J. Antonino-Daviu, "Diagnosis of Induction Motor Faults via Gabor Analysis of the Current in Transient Regime," *IEEE Trans. Instrum. Meas.*, vol. 61, no. 6, pp. 1583-1596, June 2012.

[18] F. Dalvand, A. Kalantar and M. Safizadeh, "A Novel Bearing Condition Monitoring Method in Induction Motors Based on Instantaneous Frequency of Motor Voltage," *IEEE Trans. Ind. Electron.*, vol. 63, no. 1, pp. 364-376, Jan. 2016.

[19] F. Vedreno-Santos, M. Riera-Guasp, H. Henao, M. Pineda-Sanchez and R. Puche-Panadero, "Diagnosis of Rotor and Stator Asymmetries in Wound-Rotor Induction Machines Under Nonstationary Operation Through the Instantaneous Frequency," *IEEE Trans. Ind. Electron.*, vol. 61, no. 9, pp. 4947-4959, Sept. 2014.

[20] M. Pineda-Sanchez, M. Riera-Guasp, J. Roger-Folch, J. Antonino-Daviu, J. Perez-Cruz and R. Puche-Panadero, "Diagnosis of Induction Motor Faults in Time-Varying Conditions Using the Polynomial-Phase Transform of the Current," *IEEE Trans. Ind. Electron.*, vol. 58, pp. 1428-1439, Apr. 2011.

[21] M. Pineda-Sanchez, M. Riera-Guasp, J. Antonino-Daviu, J. Roger-Folch, J. Perez-Cruz and R. Puche-Panadero, "Diagnosis of Induction Motor Faults in the Fractional Fourier Domain," *IEEE Trans. Instrum. Meas.*, vol. 59, no. 8, pp. 2065-2075, Aug 2010.

[22] E. M. K.R. Fyfe, "Analysis of Computed Order Tracking," *Mechanical Systems and Signal Processing*, vol. 11, no. 2, pp. 187-205, 1997.

[23] M. Akar, "Detection of a static eccentricity fault in a closed loop driven induction motor by using the angular domain order tracking analysis method," *Mechanical Systems and Signal Processing*, vol. 34, no. 1-2, pp. 173-182, 2013.

[24] P. Borghesani, P. Pennacchi, S. Chatterton and R. Ricci, "The velocity synchronous discrete Fourier transform for order tracking in the field of rotating machinery," Mechanical Systems and Signal Processing, vol. 44, no. 1-2, pp. 118-133, 2014.

[25] A. Sapena-Bano, M. Pineda-Sanchez, R. Puche-Panadero, J. Perez-Cruz, J. Roger-Folch, M. Riera-Guasp and J. Martinez-Roman, "Harmonic Order Tracking Analysis: A Novel Method for Fault

Diagnosis in Induction Machines," *IEEE Trans. Energy Convers*., vol. 30, no. 3, pp. 833-841, Sept. 2015.

[26] A. Sapena-Baño, J. Perez-Cruz, M. Pineda-Sanchez, J. Roger-Folch, M. Riera-Guasp and R. Puche-Panadero, "Harmonic order tracking analysis: A novel method for the diagnosis of induction generators," *Electrical Machines (ICEM), 2014 International Conference on*, Berlin, 2014, pp. 1765-1771.

[27] A. Sapena-Baño et al., "Harmonic order tracking analysis: A speed-sensorless method for condition monitoring of wound rotor induction generators in wind turbines," *Diagnostics for Electrical Machines, Power Electronics and Drives (SDEMPED), 2015 IEEE 10th International Symposium on,* Guarda, 2015, pp. 351-358.

[28] R. Puche-Panadero, M. Pineda-Sanchez, M. Riera-Guasp, J. Roger-Folch, E. Hurtado-Perez and J. Perez-Cruz, "Improved Resolution of the MCSA Method Via Hilbert Transform, Enabling the Diagnosis of Rotor Asymmetries at Very Low Slip," *IEEE Trans. Energy Convers*., vol. 24, no. 1, pp. 52-59, Mar. 2009.

[29] M. O. Mustafa, G. Nikolakopoulos, T. Gustafsson and D. Kominiak, "A fault detection scheme based on minimum identified uncertainty bounds violation for broken rotor bars in induction motors," *Control Engineering Practice* , vol. 48, pp. 63-77, 2016.

[30] T. Yang, H. Pen, Z. Wang and C. Chang, "Feature Knowledge Based Fault Detection of Induction Motors Through the Analysis of Stator Current Data," *IEEE Trans. Instrum. Meas*., vol. 65, no. 3, pp. 549-558, 2016.

[31] M. Seera and C. P. Lim, "Online Motor Fault Detection and Diagnosis Using a Hybrid FMM-CART Model," *IEEE Trans. Neural Netw. Learn. Syst.,* vol. 25, no. 4, pp. 806-812, Apr. 2014.

[32] F. Jia, Y. Lei, J. Lin, X. Zhou and N. Lu, "Deep neural networks: A promising tool for fault characteristic mining and intelligent diagnosis of rotating machinery with massive data," *Mechanical Systems and Signal Processing* , vols. 72-73, pp. 303-315, 2016.

[33] Z. Yin and J. Hou, "Recent advances on SVM based fault diagnosis and process monitoring in complicated industrial processes," *Neurocomputing*, Vols. 174, Part B, pp. 643-650, 2016.

[34] J. Hang, J. Zhang and M. Cheng, "Fault diagnosis of wind turbine based on multisensors information fusion technology," *Renewable Power Generation, IET*, vol. 8, no. 3, pp. 289-298, Apr. 2014.

[35] A. Sapena-Bano, M. Pineda-Sanchez, R. Puche-Panadero, J. Martinez-Roman and Z. Kanovic, "Low-Cost Diagnosis of Rotor Asymmetries in Induction Machines Working at a Very Low Slip Using the Reduced Envelope of the Stator Current," *IEEE Trans. Energy Convers.*, vol. 30, no. 4, pp. 1409-1419, Dec. 2015.

[36] H. Guesmi, S. B. Salem and K. Bacha, "Smart wireless sensor networks for online faults diagnosis in induction machine," *Computers & Electrical Engineering* , vol. 41, pp. 226-239, 2015.

[37] A. Bellini, F. Filippetti, G. Franceschini, C. Tassoni and G. B. Kliman, "Quantitative evaluation of induction motor broken bars by means of electrical signature analysis," in *IEEE Trans. Ind. Appl*., vol. 37, no. 5, pp. 1248-1255, Sept./Oct. 2001.

[38] M. Riera-Guasp, M. F. Cabanas, J. A. Antonino-Daviu, M. Pineda-Sánchez and C. H. R. García, "Influence of Nonconsecutive Bar Breakages in Motor Current Signature Analysis for the Diagnosis of Rotor Faults in Induction Motors," in *IEEE Trans. Energy Convers.*, vol. 25, no. 1, pp. 80-89, Mar. 2010.

**Angel Sapena-Bano** received the M.Sc. degree in Industrial Engineering and the Ph.D. degree in Electrical Engineering from the Universitat Politècnica de València (Spain) in 2009 and 2014 respectively. He is currently an Associate Professor in the Department of Electrical Engineering. His research interests focus on induction motor diagnostics and the maintenance based on the condition monitoring, numerical modeling of electrical machines, and advanced automation processes and electrical installations.

**Jordi Burriel Valencia** received his M. Sc. degree in Informatics Engineering and the Ph.D. degree in Electrical Engineering from the Universitat Politècnica de València, Spain, in 2010 and 2016, respectively. From 2012 he works as a Researcher in the Institute for Energy Engineering of Universitat Politècnica de València where he has contributed on projects related to automation systems and projects related to fault diagnosis of power transformers and turbines. Currently his research is focused on the development of expert systems for induction motors diagnosis.

**Manuel Pineda-Sanchez (M02**) received his M.Sc. degree in electrical engineering in 1985 and his Ph.D. degree in electrical engineering in 2004, both from the Universitat Politecnica de Valencia. Currently he is an Associate Professor in the Department of Electrical Engineering. His research interests include electrical machines and drives, condition monitoring of induction motors, numerical simulation of electromagnetic fields, and software development.

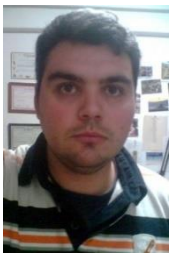

**Ruben Puche-Panadero (M09)** received his M.Sc. in Automatic and Electronic Engineering in 2003 from the Universitat Politecnica de Valencia. He received his Ph.D. in 2008 in the field of Condition Monitoring of Electrical Machines. From 2003 to 2006 he worked as a PLC programmer and as a developer of the SCADA programs. He joined to the Universitat Politecnica de Valencia in 2006 and he is currently Associate Professor of Control Electrical Machines. His research interests focus on induction motor diagnostics, numerical modeling of electrical machines, and advanced automation processes and electrical installations.

**Martin Riera-Guasp (M94-SM12)** received the M.Sc. degree in Industrial Engineering and the Ph.D. degree in Electrical Engineering from the Universitat Politecnica de Valencia (Spain) in 1981 and 1987, respectively. Currently he is an Associate Professor in the Department of Electrical Engineering of the Universitat Politecnica de Valencia. His research interests include condition monitoring of electrical machines and electrical systems efficiency.